Effective Storm-Relative Helicity and Bulk Shear in Supercell Thunderstorm Environments

RICHARD L. THOMPSON, COREY M. MEAD, AND ROGER EDWARDS

Storm Prediction Center, Norman, Oklahoma

(Manuscript received 22 August 2005, in final form 1 June 2006)

ABSTRACT

A sample of 1185 Rapid Update Cycle (RUC) model analysis (0 h) proximity soundings, within 40 km and 30 min of radar-identified discrete storms, was categorized by several storm types: significantly tornadic supercells (F2 or greater damage), weakly tornadic supercells (F0–F1 damage), nontornadic supercells, elevated right-moving supercells, storms with marginal supercell characteristics, and nonsupercells. These proximity soundings served as the basis for calculations of storm-relative helicity and bulk shear intended to apply across a broad spectrum of thunderstorm types. An effective storm inflow layer was defined in terms of minimum constraints on lifted parcel CAPE and convective inhibition (CIN). Sixteen CAPE and CIN constraint combinations were examined, and the smallest CAPE (25 and 100 J kg^{-1}) and largest CIN (-250 J kg^{-1}) constraints provided the greatest probability of detecting an effective inflow layer within an 835-supercell subset of the proximity soundings. Effective storm-relative helicity (ESRH) calculations were based on the upper and lower bounds of the effective inflow layer. By confining the SRH calculation to the effective inflow layer, ESRH values can be compared consistently across a wide range of storm environments, including storms rooted above the ground. Similarly, the effective bulk shear (EBS) was defined in terms of the vertical shear through a percentage of the "storm depth," as defined by the vertical distance from the effective inflow base to the equilibrium level associated with the most unstable parcel (maximum θ_e value) in the lowest 300 hPa. ESRH and EBS discriminate strongly between various storm types, and between supercells and nonsupercells, respectively.

1. Introduction

Supercell thunderstorm environments, from both observations and numerical simulations, typically consist of relatively large buoyancy and vertical shear through a substantial depth of the troposphere. Numerical simulations (e.g., Weisman and Klemp 1982, 1984, 1986; Weisman and Rotunno 2000) have established that strong vertical wind shear, generally greater than 20–25 m s^{-1} wind variation over the lowest 4–6 km above ground level (AGL), is necessary for the maintenance of long-lived supercell structures. Sufficient vertical shear through this depth allows for the establishment of the characteristic mesocyclone structure in right-moving supercells, such that precipitation and associated evaporative cooling do not disrupt low-level storm inflow (Weisman and Rotunno 2000; Rotunno and Weisman 2003). Though some disagreement exists regarding the influence of low-level shear versus deep-layer vertical shear in supercell propagation [e.g., the Davies-Jones (2002) and Rotunno and Weisman (2003) exchange], it is generally accepted that the primary source for midlevel rotation in supercell thunderstorms is the tilting and stretching of streamwise vorticity (Davies-Jones 1984). Davies-Jones et al. (1990) developed storm-relative helicity (hereafter SRH) as a means to quantify streamwise vorticity as a forecast tool for supercell and tornado environments.

A concern with the previous numerical simulations, and subsequent observational investigations, is that SRH calculations have been tied to somewhat arbitrary layers AGL. Predictive estimates of SRH have also relied on various storm motion algorithms (most recently Bunkers et al. 2000) in combination with approximations to the storm inflow layer (typically the lowest 1–3 km AGL). In an attempt to refine the estimates of the

Corresponding author address: Richard L. Thompson, Storm Prediction Center, 120 David L. Boren Blvd., Suite 2300, Norman, OK 73072.
E-mail: richard.thompson@noaa.gov

DOI: 10.1175/WAF969.1

storm inflow layer, the depth of the inflow layer is constrained by the vertical profiles of temperatures and moisture. Specifically, it is assumed that only lifted parcels associated with CAPE will sustain a deep thunderstorm updraft, whereas parcels associated with very large convective inhibition (CIN) will ultimately result in storm demise.[1] A sample of 1185 close proximity soundings, derived from RUC model hourly analyses, served as the basis for our estimates of the storm inflow layer.

In determining relevant bounds on a storm inflow layer, the likelihood of detecting a storm inflow layer and the error characteristics of the RUC analysis soundings both are quite important. Thompson et al. (2003, hereafter T03) compared a sample of 150 RUC analysis (0 h) and 1-h forecast soundings to observed soundings within 3 h and 185 km of observed supercells and found that the RUC soundings tended to be too cool and dry at the surface (Figs. 2a and 2b in T03). These cool and dry biases resulted in 100–250 J kg^{-1} underestimates of CAPE (after Doswell and Rasmussen 1994) in typical cases (Fig. 3 in T03), and CIN values that were too negative (not shown). Assigning a CAPE threshold too large or an absolute CIN threshold too small lowers the probability of identifying a storm inflow layer within a proximity sounding, which compounds the aforementioned RUC sounding biases. Modification of the proximity soundings with nearby surface observations counters the RUC analysis biases at the ground.

Distributions of most unstable parcel (maximum θ_e value in the lowest 300 hPa) CAPE and CIN from our 1185 proximity soundings suggested the following potential inflow layer constraints: CAPE values of 25, 100, 250, and 500 J kg^{-1}, and CIN values of -50, -100, -150, and -250 J kg^{-1} (16 possible combinations). These tested thresholds of CAPE and CIN all fell well within the lowest 10% of values for all 1185 proximity soundings, and above the minimum values of the most unstable parcel CAPE and CIN in our sample (4 and -381 J kg^{-1}, respectively).

Beginning at the ground level in each sounding and searching upward, lifted parcel CAPE and CIN values associated with each level in the sounding were compared to each of the 16 possible constraint combinations. The first level that met both of the constraints (i.e., CAPE $\geq$ 100 J kg^{-1} and CIN ≥ -250 J kg^{-1}) became the "effective inflow base." Continuing upward from the effective inflow base, the effective inflow layer consisted of all contiguous parcels that met both constraints, and the last parcel meeting the constraints became the "effective inflow top." The vertical distance between these two levels defined the effective storm inflow layer, and established the vertical bounds on the calculation of effective SRH (hereafter ESRH).

Observational studies of proximity soundings (e.g., Rasmussen and Blanchard 1998; T03) have confirmed that vertical wind shear over the lowest 6 km AGL[2] is a strong discriminator between supercell and nonsupercell thunderstorms. However, measures of vertical shear such as 0–6-km bulk vector wind difference and the bulk Richardson number (BRN) shear term represent arbitrary fixed layers. Such fixed-layer parameters become less reliable when attempting to characterize environments of storms that vary substantially from "typical" cases with an equilibrium level (EL) height near 12 km. Specific examples of very tall storms during the late spring and summer include those that hit Jarrell, Texas, on 27 May 1997 (Corfidi 1998), and Plainfield, Illinois, on 28 August 1990 (Korotky et al. 1993), with EL heights near 15 km. Storm depth can be much shallower than 12 km in association with tropical cyclone supercells (e.g., McCaul 1991; McCaul and Weisman 1996), as well as in some storm environments observed during the cool season. Also, the near-ground environment may not be relevant to storms rooted above the ground [so-called elevated thunderstorms; Colman (1990)]. As an alternative to fixed-layer shear depths, a measure of convective storm depth can define the relevant layer for vertical shear calculations (i.e., the effective inflow base to most unstable parcel EL height). In this way, vertical shear normalized to storm depth allows the consistent and potentially meaningful comparison of very tall storms, relatively shallow storms, and elevated storms, while replicating 0–6-km bulk shear in typical supercell environments. Henceforth, bulk shear normalized to a percentage of storm depth is known as the effective bulk shear[3] (EBS).

Details regarding our proximity sounding sample are discussed in section 2. Sections 3 and 4 examine ESRH and EBS, respectively, in the context of our proximity

[1] Our reference to CAPE originating in the storm inflow layer is not to be confused with parcel buoyancy *within* the inflow layer. Forced low-level (nonbuoyant) ascent is common in supercells, though lifted parcels must eventually achieve a level of free convection, or the storm will dissipate. Hence, the lifted parcels must be associated with CAPE.

[2] Weisman and Rotunno (2000) reference the hodograph length as an appropriate measure of vertical shear. However, hodograph length is sensitive to the vertical resolution (i.e., "smoothness") of the wind profile.

[3] Bulk shear refers to the magnitude of the bulk vector difference (top minus bottom) divided by depth.

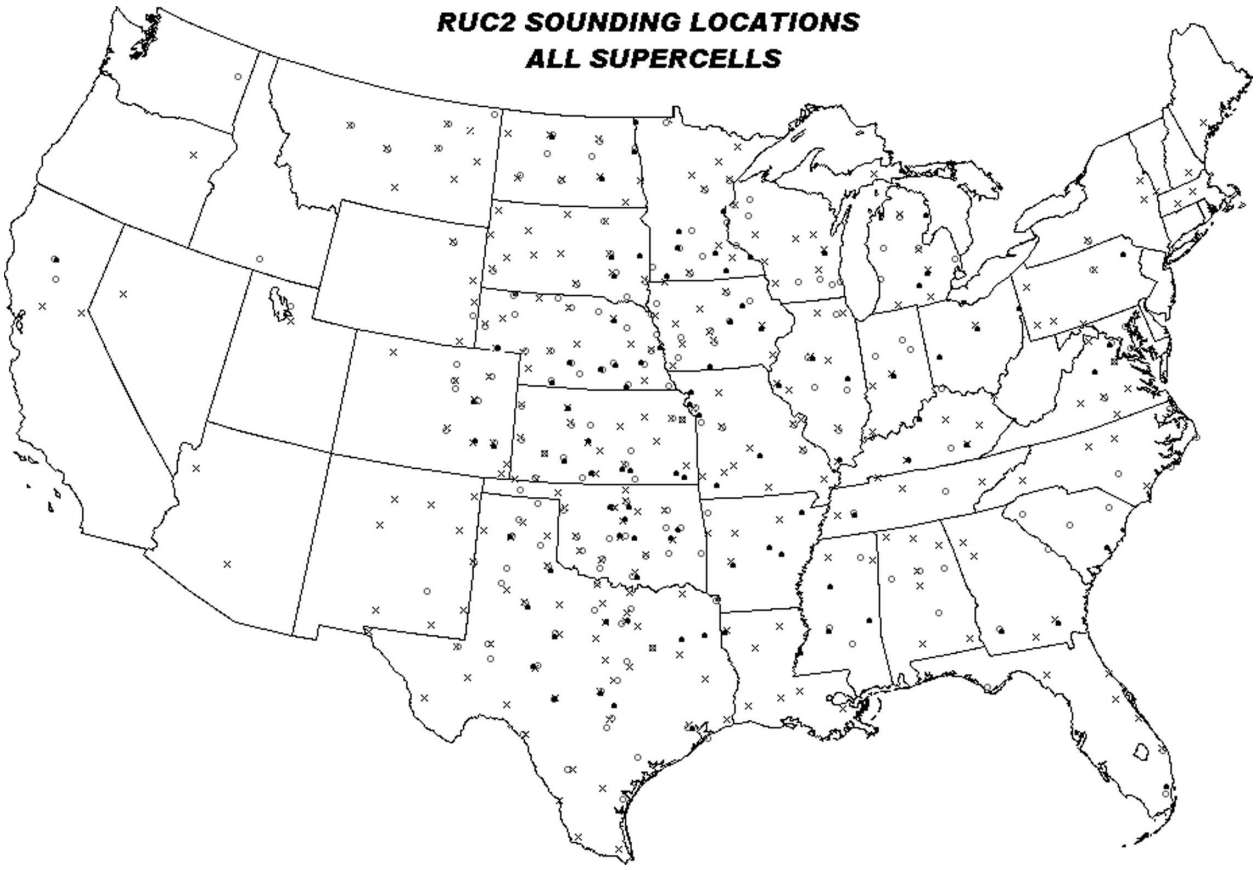

FIG. 1. RUC model proximity sounding locations for 835 supercells. Sounding locations are marked by supercell type: significantly tornadic (F2 or greater damage, solid squares), weakly tornadic (F0–F1 damage, open circles), and nontornadic (x). Multiple soundings exist for some locations marked.

sounding sample, and our findings are summarized in section 4.

2. Data and methodology

The RUC model close proximity sounding sample described in T03 has been augmented to include additional storm cases from all of 2003 through March 2005, increasing the entire sample size to 1185 soundings (835 supercells) across the conterminous United States (Fig. 1). Proximity criteria were the same as in T03 with a 0-h RUC analysis profile valid within a 40-km radius and 30 min of each radar-identified storm. This work combines the 413 close proximity soundings from T03 (25-hPa vertical resolution, interpolated from a 40-km horizontal RUC grid) with 773 newer RUC profiles (Benjamin et al. 2004) containing full model resolution in the vertical. The operational experience of the authors suggests that there has been little change in the error characteristics discussed in T03.

The following right-moving (cyclonic) supercell definitions and proximity criteria were utilized to identify proximity sounding cases during real-time data collection from April 1999 through June 2001, as well as from January 2003 through March 2005 across the conterminous United States.

1) Each candidate storm must have displayed supercell characteristics in Weather Surveillance Radar-1988 Doppler (WSR-88D) imagery for at least 30 min. Radar reflectivity structures consisted of hook echoes or inflow notches (after Browning 1964; Lemon 1977), coincident with subjective identification of cyclonic shear in velocity data. At a minimum, cyclonic (counterclockwise) azimuthal shear reached at least 0.002 s^{-1} in 1-km resolution velocity data (i.e., a peak velocity difference of 20 $m\,s^{-1}$ or greater across 10 km or less at the 0.5° or 1.5° elevation angles), similar to the mesocyclone detection algorithm described in Stumpf et al. (1998).
2) Supercells were categorized as significantly tornadic (F2 or greater tornado damage), weakly tornadic (F0–F1 tornado damage), or nontornadic. To avoid excessive influence by single days with large num-

bers of supercells, not every supercell was included in our dataset. Instead, we collected an average of roughly two cases for each day when supercells occurred. When multiple supercells of the same type occurred within a single day, only those separated by at least 3 h and 185 km became part of our dataset. Additionally, proximity soundings were collected for storms that displayed "marginal" supercell characteristics (i.e., peak cyclonic azimuthal shear less than 0.002 s^{-1}), as well as discrete storms with no supercell characteristics.

A RUC-2 analysis gridpoint sounding was generated for each 1999–2001 supercell at the analysis time closest to the most intense tornadoes with the tornadic supercells, or the time of the most significant severe weather reports with the nontornadic supercells, or at the time of the most pronounced radar signatures if no severe weather was reported. In a slight change from the T03 methodology, we collected soundings for both the initiation (within the first hour of development) and mature (≥2 h after initiation) phases of supercells, as described in Edwards et al. (2004). However, to remain consistent with T03, we considered only a single mature phase sounding for each storm case, or an initiation sounding if no mature phase sounding was available for a particular storm.

The 1999–2001 RUC-2 analysis soundings were interpolated (bilinear between the nearest four grid points) for each supercell to the closest surface observing site that was generally located upwind from the supercell at the surface, per regional observations. Surface observing sites were an option for generating soundings via the Unix version of the Skew-*T* Hodograph Analysis and Research Program (NSHARP; Hart and Korotky 1991) software, which allowed relatively simple identification of each case. The RUC-2 analysis grids were available at 40-km horizontal grid spacing, on isobaric surfaces with 25-hPa vertical resolution (e.g., 1000, 975, 950, 925 hPa, etc.). Proximity soundings for 2003–2005 consisted of the full model resolution in the vertical. Soundings were generated at fixed locations, though the same proximity criteria from T03 were retained. The coverage of the 2003–2005 proximity sounding locations was greatest in the eastern United States (Fig. 2), and somewhat less across portions of the high plains and Intermountain West. The gaps in sounding coverage may have introduced a small underrepresentation of high plains supercell cases, while the relative lack of proximity soundings across the western states was attributable largely to a lack of candidate supercell events.

Observed storm motions were derived from mean 1-h motions of radar echo centroids. Observed temperatures and dewpoint temperatures at the closest surface observing site were also collected for each proximity sounding, with observations interpolated between sites for a few of the 1999–2001 soundings. These observations were used to modify the surface conditions for each sounding, given that the largest errors in the RUC analysis soundings tended to be at the ground, per T03. Model sounding levels above the ground were not modified owing to a paucity of real-time observational data off the surface in the majority of cases.

a. Effective SRH

The effective inflow base and top defined the layer for the effective SRH calculation. Four CAPE thresholds (25, 100, 250, and 500 J kg^{-1}) and four CIN thresholds (−50, −100, −150, and −250 J kg^{-1}) were tested in 16 combinations as potential bounds on the effective inflow layer (Table 1). The least stringent parcel constraints (e.g., 25 and 100 J kg^{-1} CAPE with −250 J kg^{-1} CIN) resulted in the highest probabilities of detecting a nonzero effective inflow layer depth (0.96 and 0.95, respectively) for our 835 supercell proximity soundings. *Given the importance of the probability of detection and some concern for false alarms in operational forecasting of supercell environments, the 100 J kg^{-1} CAPE and −250 J kg^{-1} CIN constraints were chosen to represent the bounds of the effective inflow layer.*

The sounding displayed in Fig. 3 was associated with an elevated, right-moving supercell in an environment with no surface-based CAPE, but a most unstable parcel CAPE of 1350 J kg^{-1}. The dark horizontal lines to the left of the temperature and moisture profiles, marked at 900 and 650 hPa, denote the base and top of the effective inflow layer, based on a lifted parcel CAPE ≥ 100 J kg^{-1} and CIN ≥ −250 J kg^{-1}. For these CAPE and CIN constraints, the effective inflow layer in Fig. 3 begins at 699 m above model ground level, and extends upward to 3395 m above model ground level, resulting in an inflow layer depth of 2696 m. The fixed-layer 0–3-km SRH for this supercell case was 356 $m^2 s^{-2}$ (observed storm motion), while the ESRH was reduced to 88 $m^2 s^{-2}$ (see Fig. 4). Exclusion of the relatively dry and stable layer from the ground to 900 hPa resulted in a reduced ESRH value in comparison to the 0–3-km SRH.

b. Effective bulk shear

The EL height (based on the maximum θ_e value in the lowest 300 hPa) for each proximity sounding defined the upper bound to the storm depth. The lower bound to storm depth was defined as the effective in-

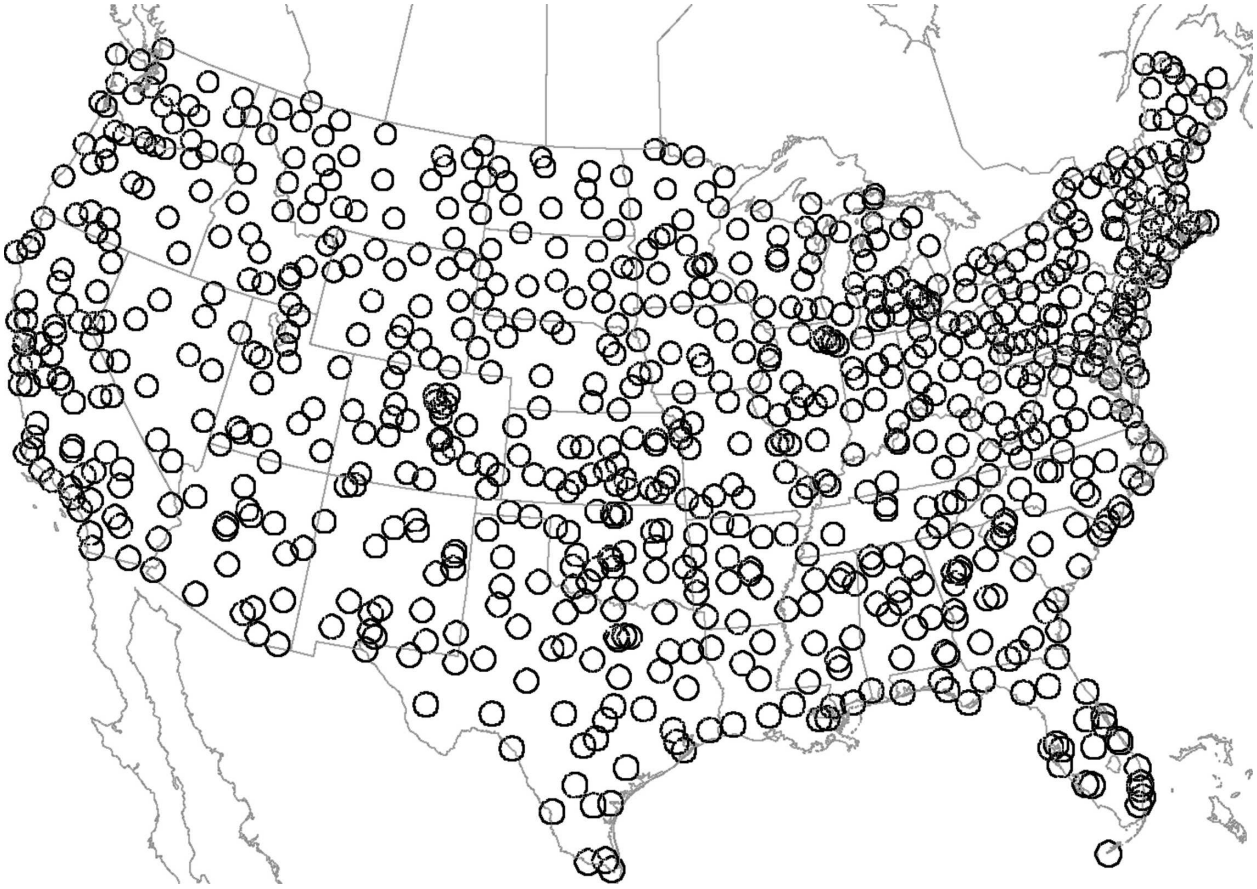

FIG. 2. RUC model point forecast sounding sites used in the identification of supercell proximity sounding cases from 2003 through March 2005. The range rings denote the proximity sounding radius of 40 km around each site.

flow base, as discussed previously. Bulk vertical shear was calculated for 10 equally deep layers between the effective inflow base and the EL. For example, the bottom of the effective inflow layer (699 m AGL) marks the "base" of the storm in Fig. 3, while the EL (~205 hPa or 11 736 m AGL) marks the "top" of the storm. Translating this effective storm depth to a hodograph, the EBS vector for the lower half of the storm depth is shown in Fig. 5 (this choice is described in more detail in section 3b). Note that the effective bulk wind difference [EBWD, 57 kt (29 m s^{-1})] is larger than the standard 0–6-km bulk wind difference [BWD, 47 kt (24 m s^{-1})] in this example, while the orientation of the EBS vector is toward the south, as opposed to a northwest to southeast orientation for the 0–6-km bulk shear vector. Considering the depth of the layer in each calculation, the 0–6-km bulk shear vector and the EBS vector convert to 0.004 and 0.005 s^{-1}, respectively.

c. Storm motion estimates

In anticipation of operational applications of the ESRH and EBS techniques, we explored modifications to the "internal dynamics (ID) method" supercell motion algorithm developed by Bunkers et al. (2000), with specific interest in improving storm motion estimates for storms not rooted near the ground. The ID method relies on estimating two components of storm motion: advection by a mean wind, and storm propagation based on the vector shear through a portion of the storm depth. Both components were examined by Bunkers et al. (2000), and storm motion errors were minimized for the mean wind and vector shear through the lowest 6 km AGL. However, all of the supercells in the

TABLE 1. Proportions of supercell proximity soundings (835) with nonzero effective inflow layer depth for 16 combinations of CAPE and CIN constraints (J kg^{-1}).

		CIN			
		−250	−150	−100	−50
CAPE	25	0.96	0.89	0.84	0.72
	100	0.95	0.88	0.84	0.71
	250	0.91	0.85	0.84	0.69
	500	0.88	0.83	0.78	0.65

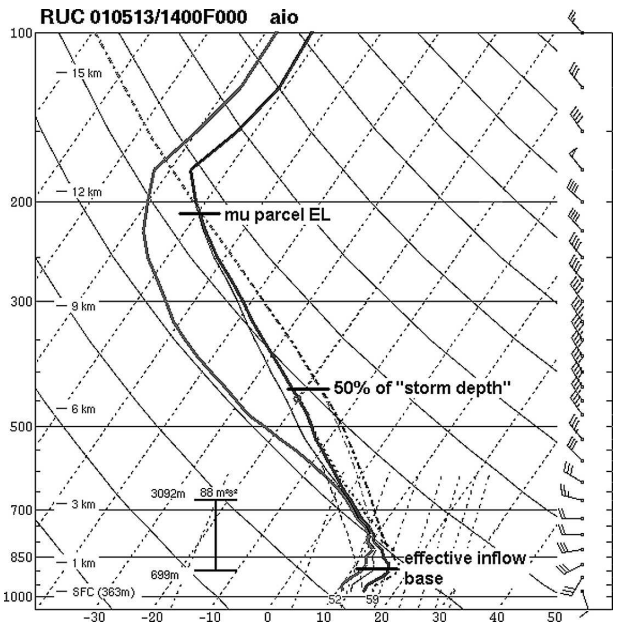

FIG. 3. Skew *T*–log*p* plot of a RUC model proximity sounding for an elevated right-moving supercell from 13 May 2001 at 1400 UTC. Heavy horizontal lines across the temperature and dewpoint profiles represent the effective inflow base, the most unstable (mu) parcel EL height, and 50% of the depth from the effective inflow base to mu parcel EL height ("storm depth"). Left of the sounding plot, the effective inflow layer, using parcel constraints of CAPE ≥ 100 J kg^{-1} and CIN ≥ -250 J kg^{-1}, is marked by the vertical bar in the lower-left portion of the diagram, with heights AGL marked. Additionally, the effective SRH value for this sounding is plotted above the bar. The dashed parcel ascent paths represent the (left) nonvirtual and (right) virtual temperature correction, though only the virtual parcel ascent is used in any calculations. Heights in AGL are noted along the left side of the diagram.

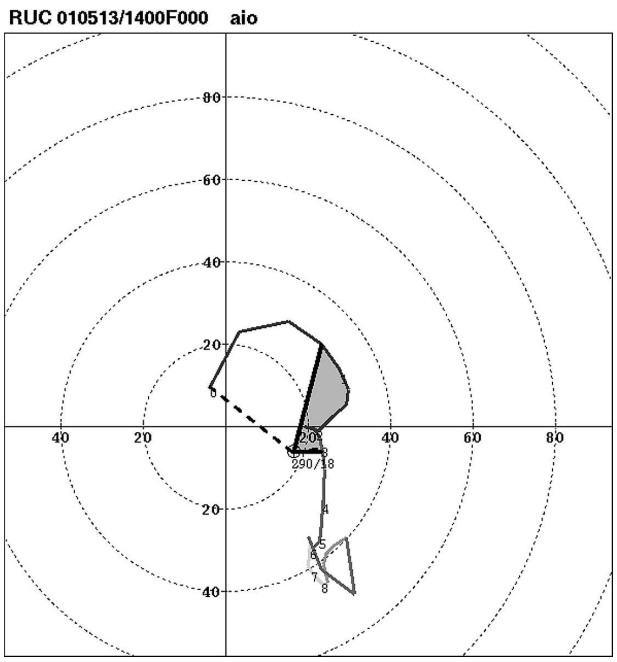

FIG. 4. Hodograph illustration of the effective SRH for the same elevated supercell case presented in Fig. 3. The shaded area is proportional to the effective SRH (observed storm motion), while the heavy dashed lines enclose the area proportional to the 0–3-km SRH. Heights in km AGL are noted along the plotted wind profile, and range rings mark the ground-relative wind speeds in 20-kt (10 m s^{-1}) increments.

Bunkers dataset were surface based, which brings into question the utility of the ID method in elevated supercell cases where the storms can be decoupled vertically from the near-ground environment.

Recently, Ramsay and Doswell (2005, hereafter RD05) examined five supercell motion techniques with a sample of 394 observed proximity soundings. They found that the ID method, modified to use the 0–8-km mean wind, produced the smallest mean vector errors. We proposed additional changes to the original ID method, such as replacement of the fixed-layer mean wind and bulk shear with the effective bulk vector shear and mean wind through the lower half of the storm depth. The mean wind over the lower 67% of the storm depth was included in a separate version of the ID method, where 8 km AGL represents 67% of our median EL height of 12 010 m AGL. These three modified ID methods, and the original ID method, were tested on all 835 supercells in our sample.

The original ID method resulted in the smallest mean absolute error (4.6 m s^{-1}), our two ID modifications scaled to storm depth both produced mean absolute errors near 4.8 m s^{-1}, and the RD05 modification to the ID method resulted in the largest mean absolute error (4.9 m s^{-1}). Mean absolute error was reduced by about 2 m s^{-1} with our modified (lower half of storm depth) ID method for a small subset of supercells based well above the ground (i.e., effective inflow base greater than 750 m AGL), though the sample size is too small to draw meaningful conclusions. Our findings are in general agreement with those of RD05 in that storm motion estimates did not improve when normalizing the shear and mean wind calculations to storm depth.

3. Results

a. Effective SRH

Calculations of SRH in supercell environments have been based typically on a fixed layer (e.g., 0–3 km above ground level) and an assumed storm motion estimate that was developed from a sample of surface-based supercells (e.g., the ID method). This typical approach brings into question the representativeness of

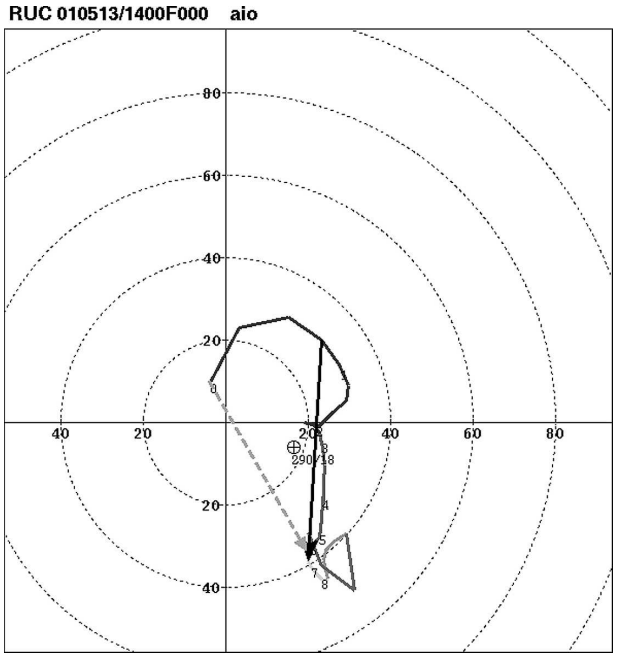

FIG. 5. Hodograph plot of the wind profile (kt, light gray) associated with the sounding shown in Fig. 3. The hodograph is annotated with the effective bulk shear vector (solid black) through the lowest half of the "storm depth" (see Fig. 3), and the 0–6-km bulk shear vector (dashed gray). Hodograph conventions are the same as in Fig. 4.

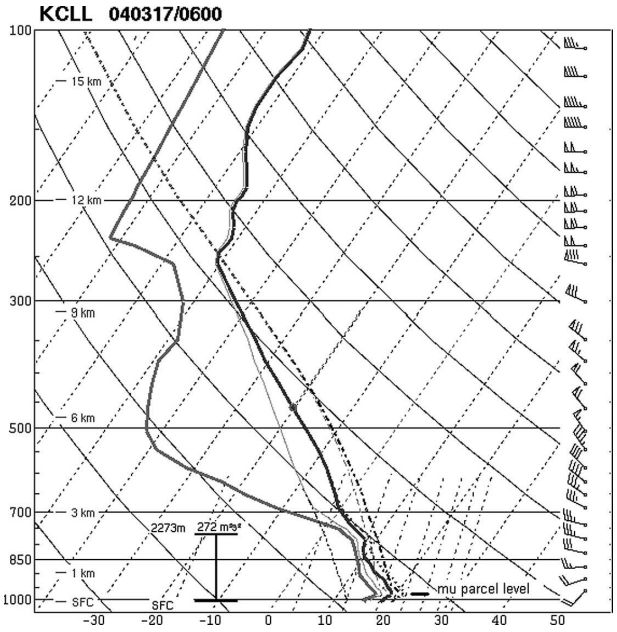

FIG. 6. Skew T–log$p$ plot of a RUC model proximity sounding displaying both an effective inflow layer base at the ground and a most unstable parcel level above the ground. The most unstable (mu) parcel level height is marked with a heavy horizontal line to the right of the sounding plot. Other plotting conventions are the same as in Fig. 3.

0–1 or 0–3 km as the "inflow" layer for most supercells, particularly in the special case of an elevated supercell. SRH is likely overestimated for elevated storms by including vertical shear in the near-ground layer that is decoupled vertically from the storm (e.g., instability based above a stable surface layer, as shown in Fig. 3).

The most obvious elevated supercell environment can be defined as an effective inflow base above the ground. However, there are cases where a supercell can be considered somewhat elevated when the most unstable parcel originates above the ground, but the effective inflow base is the ground level (Fig. 6). This situation is similar to the "large CIN–high level of free convection (LFC)" environments discussed by Davies (2004). Here, a supercell is defined as elevated when the effective inflow base is above the ground in the associated proximity sounding.

It is important to note that in some cases an effective inflow layer was not identified; thus, ESRH could not be calculated and was assumed to be zero. An effective inflow layer can be missing from a sounding for the following reasons:

1) insufficient buoyancy (CAPE < 100 J kg^{-1} for all lifted parcels),
2) excessive convective inhibition (CIN < -250 for all lifted parcels), or
3) the effective inflow "layer" is a single level in the sounding. This scenario is often associated with modifying the RUC sounding for the observed surface conditions, while the cool and dry biases in the RUC analyses result in the next level above the ground not meeting the effective inflow layer constraints.

Figure 7 suggests that the depth of the effective inflow layer varies little across a spectrum of storm types, though the elevated right-moving supercells are associated with somewhat shallower inflow layers in the cases with lesser CAPE (e.g., the lowest quartile in Fig. 7 for the elevated nontornadic supercells). Interestingly, effective layer depths (which begin at the ground for all but 10 weakly tornadic supercells and 45 elevated nontornadic supercells) were typically between the standard 0–1- and 0–3-km SRH layers. Effective inflow layer depths with the elevated nontornadic supercells were similar to those with the surface-based nontornadic supercells, though effective inflow bases ranged from just above the ground to in excess of 2 km AGL in the elevated cases.

ESRH decreases markedly from the significantly tornadic supercells to the nontornadic supercells (Fig. 8), while the ESRH with elevated nontornadic supercells resembles the values associated with nontornadic su-

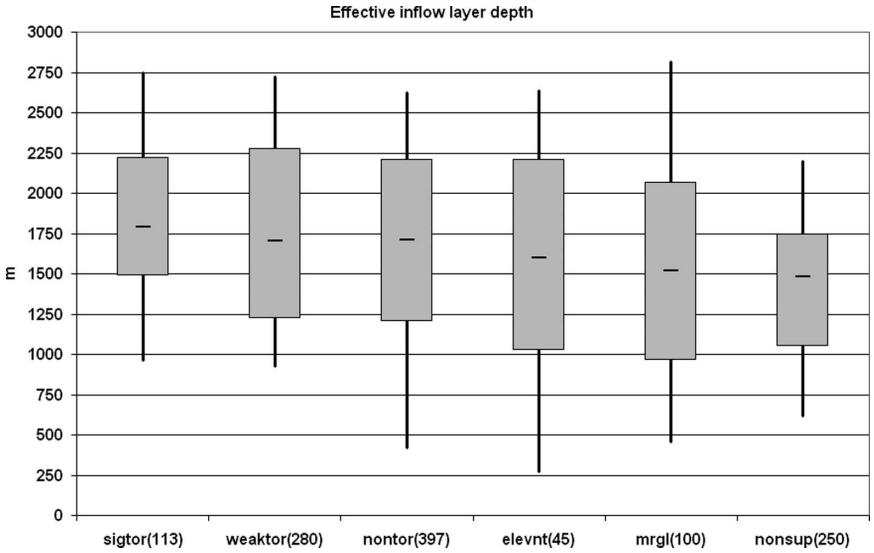

FIG. 7. Box and whiskers plots of effective layer depth (m) for the CAPE ≥ 100 J kg^{-1} and CIN ≥ -250 J kg^{-1} parcel constraints for the following groups of discrete storms: significantly tornadic (sigtor), weakly tornadic (weaktor), nontornadic (nontor), elevated nontornadic (elevnt), marginal supercells (mrgl), and nonsupercells (nonsup). The shaded boxes enclose the 25th percentile (bottom of box) to the 75th percentile values, with the median values are marked by a horizontal dash within each box. The whiskers extend upward to the 90th percentiles, and downward to the 10th percentiles. Sounding sample sizes are given in parentheses.

percells. The effective inflow base was above the ground in 10 of our 280 weakly tornadic cases (4%), though the reported tornadoes with these storms tended to be single, short-lived events. The ability to discriminate between significantly tornadic, weakly tornadic, and nontornadic supercells with ESRH is not particularly sensitive to the specific CAPE and CIN thresholds tested, though the effective inflow layer depth and resultant ESRH values tend to be reduced with the more stringent parcel constraints (not shown).

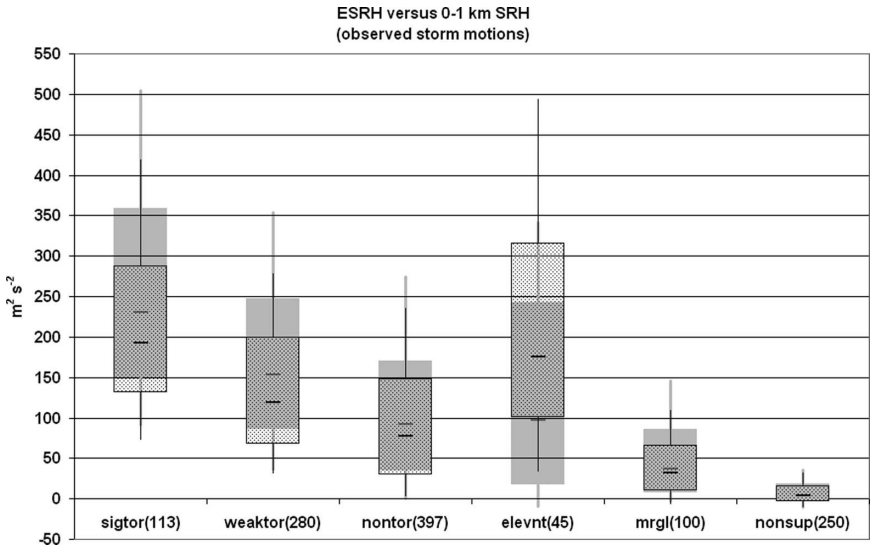

FIG. 8. Box and whiskers overlay plots of effective SRH (m^2 s^{-2}) based on the CAPE ≥ 100 J kg^{-1} and CIN ≥ -250 J kg^{-1} parcel constraints (solid gray box and thick gray whiskers), and 0–1-km SRH (dotted black box and thin black whiskers). Plotting conventions are the same as in Fig. 7.

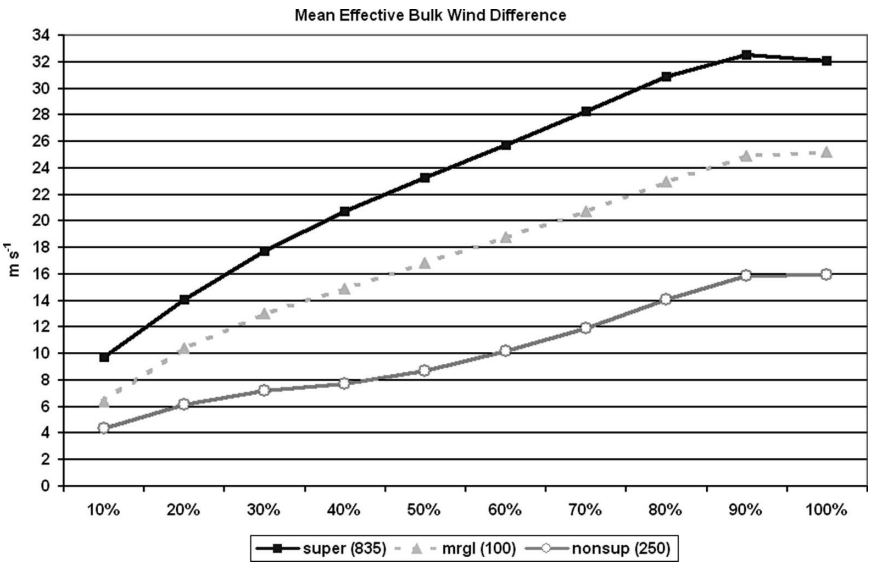

FIG. 9. Mean EBWD ($m\ s^{-1}$) by percentage of storm depth. All supercells are denoted by "super" in the legend, and other storm group conventions are the same as in Fig. 7.

In comparing SRH calculations for the effective inflow layers and the fixed 0–1-km layer (Fig. 8), ESRH discriminates a little more clearly between the classes of surface-based supercells. The parcel constraints of CAPE $\geq 100\ J\ kg^{-1}$ and CIN $\geq -250\ J\ kg^{-1}$ are not so harsh as to mask elevated supercell environments with relatively small CAPE, but are sufficient to remove the influence of inflow parcels characterized by excessive CIN and/or minimal CAPE.

Of particular interest in Fig. 8 is the large variation in SRH between the fixed 0–1-km layer and the effective inflow layer for the elevated right-moving supercells. Elevated supercells are relatively common in lower-tropospheric warm advection regimes, which often are associated with substantial CAPE based above the ground. The fixed 0–1-km layer includes the impact of the near-ground layer, which tends to be characterized by large vertical shear but little or no positive buoyancy in these regimes (refer to Fig. 3). However, ESRH only considers the inflow layer associated with some CAPE and without excessive CIN. Therefore, ESRH appears to provide a more reasonable estimate of the SRH within elevated supercell environments. Similarly, the other five storm groups reveal a consistent reduction in SRH from the 0–3-km layer to the effective inflow layer (not shown), because the effective inflow layer rarely extends a depth of 3 km AGL (refer to Fig. 6).

b. Effective bulk shear

The EBWD corresponds to the familiar 0–6-km bulk wind difference that is often referenced in operational forecast products originating from the Storm Prediction Center and local National Weather Service offices. The EBWD tends to increase through the depth of the storm for both supercells and nonsupercells, though it usually is much larger for the supercells (Fig. 9). Not surprisingly, the EBWD associated with storms displaying "marginal" supercell characteristics tends to fall between that of the supercells and discrete nonsupercell storms.

An alternative view of the EBWD is shown in Fig. 10 in the form of a line plot derived from percentile rank distributions for the different storm groups. Line segments trace the weaker EBWD values (10th percentile) with the supercells and the stronger EBWD values (90th percentile) with nonsupercells for each 10% of storm depth, allowing for an uncluttered comparison of 20 box and whisker plots (every 10% of storm depth for the two storm groups). The nonsupercell values are larger than the supercell values in Fig. 10 in the lower potions (10%–30%) and upper portions (70%–100%) of storm depth, suggesting substantial overlap in the EBWD distributions. However, the nonsupercell 90th percentile values are smaller than the supercell 10th percentile values through the middle portions (40%–60%) of the storm depth. This suggests that the difference between supercells and nonsupercells is most pronounced through the middle portions of the storms, with 50% of the storm depth representing the midpoint of the layer with the greatest difference between supercells and nonsupercells. The EBWD over the lower 50% of the storm depth discriminates strongly between

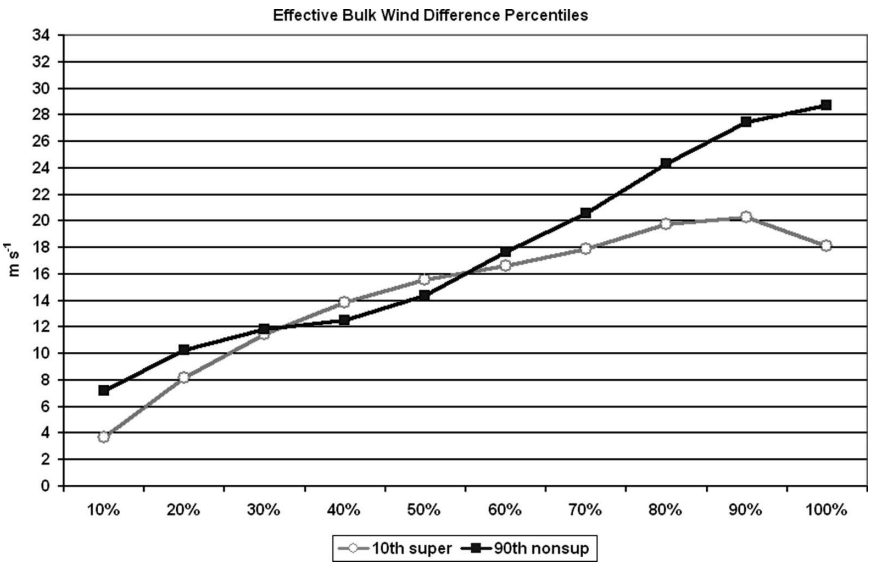

FIG. 10. Selected percentile rank plots of EBWD (m s^{-1}) by percentage of storm depth. The lines plotted are 10th percentile for surface-based, right-moving supercells (black, square markers), and the 90th percentile for nonsupercells (gray, open circle markers). Other figure conventions are the same as in Fig. 9.

supercell and nonsupercell storms (Fig. 11). However, the differences between the tornadic and nontornadic supercells are quite small, which suggests that EBWD is most suitable as a supercell diagnostic parameter. The EBWD through the lower 50% of the storm depth, divided by half of the storm depth, represents a true physical measure of vertical shear and is hereafter referred to as the EBS.

The EBS is quite similar to the 0–6-km AGL bulk shear for most of the surface-based storms in our sample whose EL heights range from 11 to 13 km AGL. The original sounding used in the Weisman and Klemp (1982) numerical simulations depicted an EL height of ~11 300 m AGL (see the 14 g kg^{-1} surface lifted parcel trace in their Fig. 1). The 0–6-km bulk shear represents the lowest ~55% of the storm depth in their sounding,

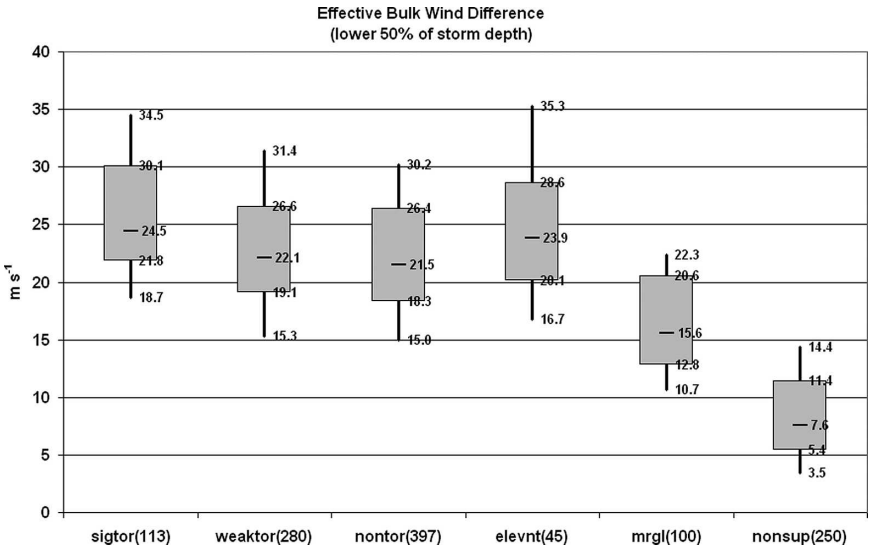

FIG. 11. Box and whiskers plot of EBWD (m s^{-1}, lower 50% of storm depth) for each group of discrete storms. Figure conventions are the same as in Fig. 7, with specific percentile values along the right side of each box and whisker.

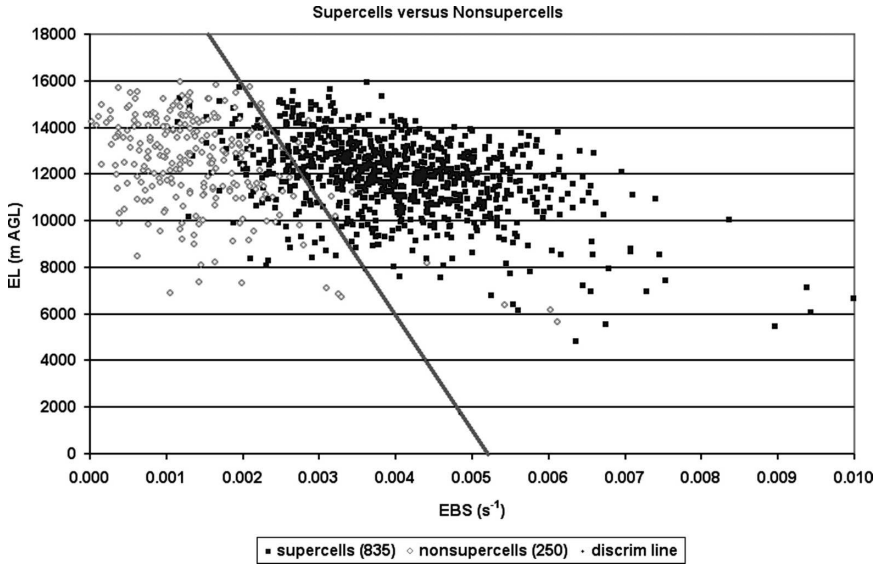

FIG. 12. Scatterplot of EL height vs EBS for 835 supercells (solid black squares) and 250 nonsupercells (open gray squares). A linear discriminant function is plotted (solid gray) that correctly separates the supercells (right of the line) from the nonsupercells (left of the line) in 89% of the cases.

which falls near the depth of the EBS (i.e., 5650 m AGL for the Weisman and Klemp sounding). The EBS discriminates strongly between supercell and nonsupercell storms, similar to the 0–6-km bulk shear (not shown). Based on linear discriminant analysis (Wilks 1995), 89% percent of our storm cases can be correctly identified as supercells or nonsupercells through the use of just the EBS and EL height (see Fig. 12).

Differences between the fixed-layer and effective-layer approaches become more apparent when comparing surface-based supercell and elevated supercell soundings (Fig. 13). The 0–6-km bulk shear is nearly identical to the EBS for the surface-based supercells, which consist of EL heights in a narrow range near 12 km. However, the 0–6-km bulk shear is weaker than the EBS for the elevated supercells. This result may seem counterintuitive given that the 0–6-km bulk shear includes the near-ground layer, which often contains

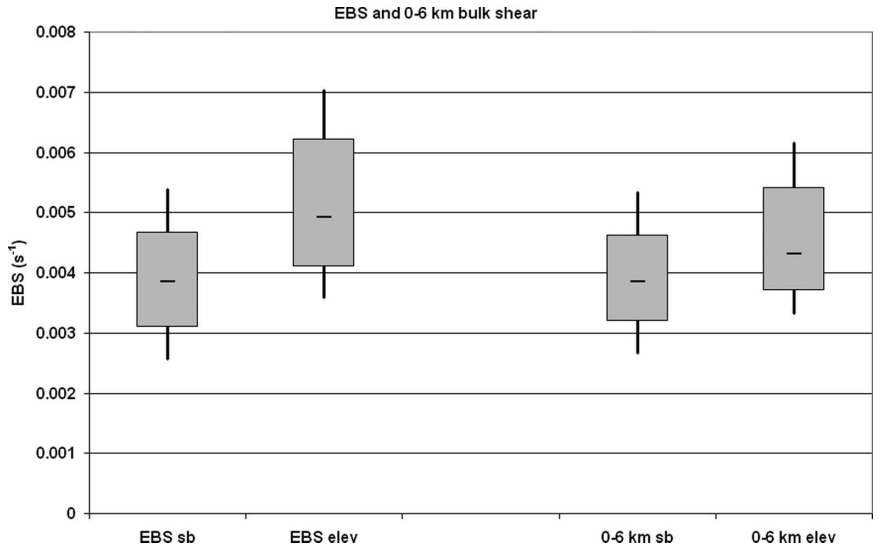

FIG. 13. Box and whiskers plots of EBS and 0–6-km shear for 780 surface-based supercells (sb) and 55 elevated supercells (elev). Other conventions are the same as in Fig. 7.

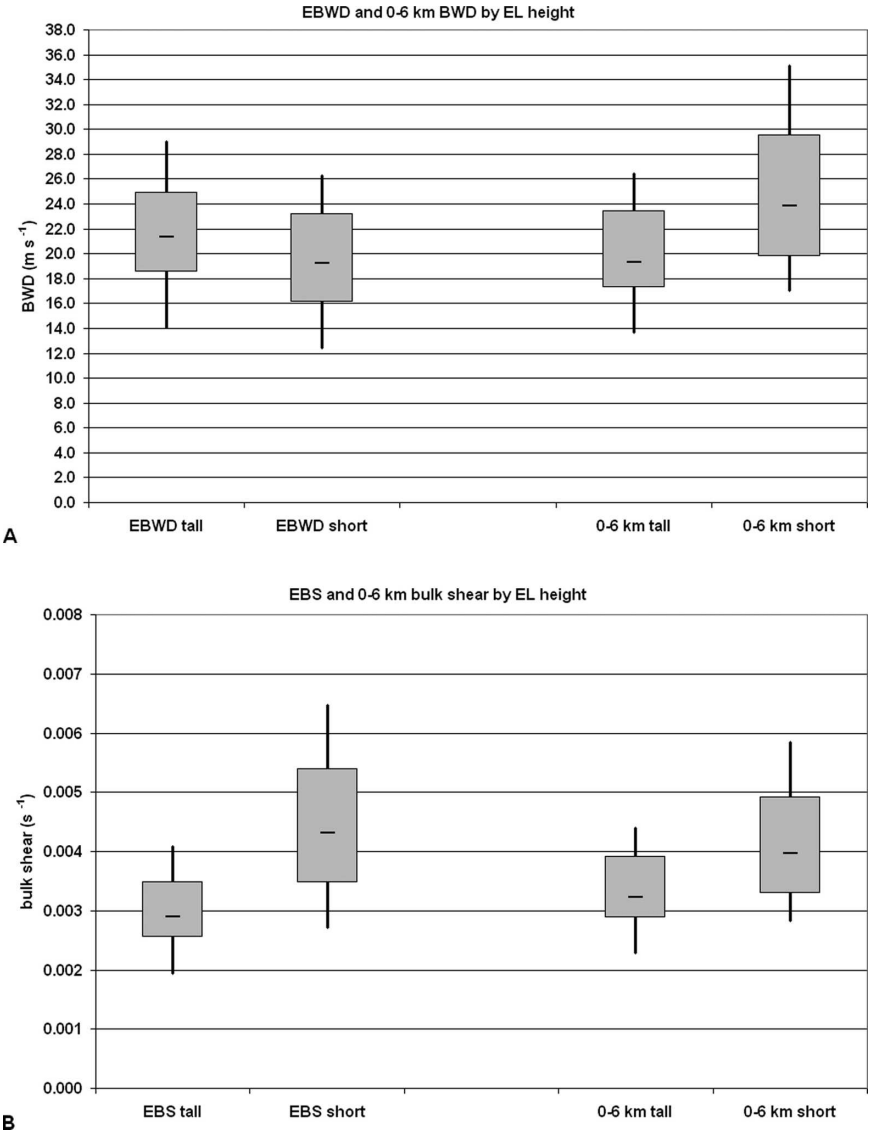

FIG. 14. Box and whiskers plots of (a) EBWD (left) and 0–6-km BWD (right), and (b) EBS (left) and 0–6-km bulk shear (right) for two equal size groups (78 soundings) of supercells. The "tall" storms represent the highest 10% of EL heights, and the "short" storms are the lowest 10% of EL heights. The EL heights are based on the maximum θ_e value in the lowest 300 hPa, and other conventions are the same as in Fig. 7.

large vertical shear in elevated thunderstorm environments, while the EBS extends to only the effective inflow base (above the ground). The EBWD tends to be smaller than the 0–6-km BWD, but the shallower depths of the elevated storms compensate to the extent that EBS is greater than the 0–6-km bulk *shear*.

Another concern with fixed-layer shear calculations is when a storm is particularly tall or short. For example, the 0–6-km bulk shear represents only the bottom 35%–45% of the highest EL case storm depths in our supercell sample, but it extends through 65%–95% of the storm depth in our lowest EL cases. The 0–6-km differences between the BWD and the EBWD are highlighted via a comparison of the tallest and shortest storm depth cases in our proximity sounding sample (Fig. 14a). The fixed-layer 0–6-km calculation results in larger BWD values with the shortest supercells compared to the tallest supercells, which is attributable to calculating the BWD through a greater percentage of storm depth in the shortest versus the tallest storms. However, the EBWD calculation provides an intuitive result in that the EBWD is smaller for the shortest

supercells. This difference in the techniques is reversed, however, when considering the actual bulk *shear* through the storm depth. As shown in Fig. 14b, the EBS approach has a larger impact on the bulk shear values associated with the shortest supercells. The EBS values are substantially larger with the shortest supercells (78 cases with EL heights $<$ 9903 m AGL), and slightly smaller with the tallest storms (78 cases with EL heights $>$ 13 892 m AGL). The EBS has a greater impact on the shorter storms because the depth of the shear calculation is much less compared to that of the tallest storms. EBS depth varies from ~7900 m AGL in the tallest storms to ~3000 m in the shortest storms. For bulk vertical shear to be equal in the tall and short storm cases, the bulk wind difference must be 225% larger in the tall storm relative to the short storm [EBWD of 17.5 m s^{-1} (34 kt) and 39.5 m s^{-1} (77 kt) for the short and tall storm examples, respectively]. An explanation for the larger impact on the shortest storms, as compared to the tallest storms, is that the shortest storms have EL heights 50%–80% of the median EL height in our sample (12 011 m AGL), while the tallest storms have EL heights only 115%–135% of the median storm (i.e., the distribution is not Gaussian).

4. Summary and conclusions

A technique to define the inflow layer of a thunderstorm, in terms of constraints on lifted parcel CAPE and CIN values, was developed and tested on a sample of 1185 close proximity soundings derived from RUC model analyses, after T03. This sounding technique, identified as the effective inflow layer, was applied to calculations of SRH with the intent of replacing fixed-layer SRH calculations. Results of this approach suggest that the ESRH more clearly discriminates between significantly tornadic and nontornadic supercells than the standard 0–1- and 0–3-km fixed-layer versions of SRH (see Rasmussen and Blanchard 1998). The effective inflow layer also allows calculation of a more meaningful SRH for elevated thunderstorms by omitting layers in a sounding that are unlikely to contribute to storm updraft maintenance because of either excessive CIN or insufficient lifted parcel CAPE. Our results suggest that the ESRH (based on a parcel CAPE $\geq$ 100 J kg^{-1} and CIN ≥ -250 J kg^{-1}) can be used to identify environments favoring both surface-based and elevated right-moving supercells.

The concept of the effective inflow layer was extended to include estimates of bulk vertical shear through the "storm depth." This EBS technique, much like the fixed-layer 0–6-km AGL bulk shear, discriminates strongly between supercell and nonsupercell thunderstorms. The use of the effective inflow base in the EBS calculation also allows elevated supercell environments to be treated similarly to surface-based storm environments, while identifying the vertical shear relevant to elevated storms. The EBS normalizes the shear values for shallow and very tall storms, allowing more realistic assessments of these storm profiles. Still, the dynamical impact of vertical shear scaled to storm depth is not known, and may require a series of numerical simulations to diagnose the role of vertical shear in storm environments that vary substantially from typical supercell environments with EL heights near 12 km AGL.

Acknowledgments. The authors thank Steve Weiss, David Bright, Pete Banacos, and Steve Goss of the SPC for their thought-provoking reviews of this manuscript, and John Hart for his programming assistance with the early versions of our calculations. Special thanks to Jon Davies for several suggested improvements to the original manuscript, and for his willingness to discuss various stages of this work. Mike Coniglio (NSSL) assisted with the linear discriminant analysis applied to Fig. 12. The thorough efforts of three anonymous reviewers led to substantial improvements in the manuscript.

REFERENCES

Benjamin, S. G., and Coauthors, 2004: An hourly assimilation–forecast cycle: The RUC. *Mon. Wea. Rev.,* **132,** 495–518.

Browning, K. A., 1964: Airflow and precipitation trajectories within severe local storms which travel to the right of the winds. *J. Atmos. Sci.,* **21,** 634–639.

Bunkers, M. J., B. A. Klimowski, J. W. Zeitler, R. L. Thompson, and M. L. Weisman, 2000: Predicting supercell motion using a new hodograph technique. *Wea. Forecasting,* **15,** 61–79.

Colman, B. R., 1990: Thunderstorms above frontal surfaces in environments without positive CAPE. Part I: A climatology. *Mon. Wea. Rev.,* **118,** 1103–1122.

Corfidi, S. F., 1998: Some thoughts on the role mesoscale features played in the 27 May 1997 central Texas tornado outbreak. Preprints, *19th Conf. on Severe Local Storms,* Minneapolis, MN, Amer. Meteor. Soc., 177–180.

Davies, J. M., 2004: Estimations of CIN and LFC associated with tornadic and nontornadic supercells. *Wea. Forecasting,* **19,** 714–726.

Davies-Jones, R. P., 1984: Streamwise vorticity: The origin of updraft rotation in supercell storms. *J. Atmos. Sci.,* **41,** 2991–3006.

——, 2002: Linear and nonlinear propagation of supercell storms. *J. Atmos. Sci.,* **59,** 3178–3205.

——, D. W. Burgess, and M. Foster, 1990: Test of helicity as a tornado forecast parameter. Preprints, *16th Conf. on Severe Local Storms,* Kananaskis Park, AB, Canada, Amer. Meteor. Soc., 588–592.

Doswell, C. A., III, and E. N. Rasmussen, 1994: The effect of neglecting the virtual temperature correction on CAPE calculations. *Wea. Forecasting,* **9,** 625–629.

Edwards, R., R. L. Thompson, and C. M. Mead, 2004: Assessment of anticyclonic supercell environments using close proximity soundings from the RUC model. Preprints, *22d Conf. on Severe Local Storms,* Hyannis, MA, Amer. Meteor. Soc., CD-ROM, P1.2.

Hart, J. A., and W. Korotky, 1991: The SHARP workstation v1.50 users guide. National Weather Service, 30 pp. [Available from NWS Eastern Region Headquarters, 630 Johnson Ave., Bohemia, NY 11716.]

Korotky, W., R. W. Przybylinski, and J. A. Hart, 1993: The Plainfield, Illinois, tornado of August 28, 1990: The evolution of synoptic and mesoscale environments. *The Tornado: Its Structure, Dynamics, Prediction and Hazards, Geophys. Monogr.,* Vol. 79, Amer. Geophys. Union, 611–624.

Lemon, L. R., 1977: New severe thunderstorm radar identification techniques and warning criteria: A preliminary report. NOAA Tech. Memo. NWS NSSFC-1, 60 pp.

McCaul, E. W., Jr., 1991: Buoyancy and shear characteristics of hurricane-tornado environments. *Mon. Wea. Rev.,* **119,** 1954–1978.

——, and M. L. Weisman, 1996: Simulations of shallow supercell storms in landfalling hurricane environments. *Mon. Wea. Rev.,* **124,** 408–429.

Ramsay, H. A., and C. A. Doswell III, 2005: A sensitivity study of hodograph-based methods for estimating supercell motion. *Wea. Forecasting,* **20,** 954–970.

Rasmussen, E. N., and D. O. Blanchard, 1998: A baseline climatology of sounding-derived supercell and tornado parameters. *Wea. Forecasting,* **13,** 1148–1164.

Rotunno, R., and M. L. Weisman, 2003: Comments on "Linear and nonlinear propagation of supercell storms." *J. Atmos. Sci.,* **60,** 2413–2419.

Stumpf, G. J., A. Witt, E. D. Mitchell, P. L. Spencer, J. T. Johnson, M. D. Eilts, K. W. Thomas, and D. W. Burgess, 1998: The National Severe Storms Laboratory mesocyclone detection algorithm for the WSR-88D. *Wea. Forecasting,* **13,** 304–326.

Thompson, R. L., R. Edwards, J. A. Hart, K. L. Elmore, and P. M. Markowski, 2003: Close proximity soundings within supercell environments obtained from the Rapid Update Cycle. *Wea. Forecasting,* **18,** 1243–1261.

Weisman, M. L., and J. B. Klemp, 1982: The dependence of numerically simulated convective storms on vertical wind shear and buoyancy. *Mon. Wea. Rev.,* **110,** 504–520.

——, and ——, 1984: The structure and classification of numerically simulated convective storms in directionally varying wind shears. *Mon. Wea. Rev.,* **112,** 2479–2498.

——, and ——, 1986: Characteristics of isolated convective storms. *Mesoscale Meteorology and Forecasting,* P. S. Ray, Ed., Amer. Meteor. Soc., 331–358.

——, and R. Rotunno, 2000: The use of vertical wind shear versus helicity in interpreting supercell dynamics. *J. Atmos. Sci.,* **57,** 1452–1472.

Wilks, D. S., 1995: *Statistical Methods in the Atmospheric Sciences*. Academic Press, 467 pp.